

ORIGINAL RESEARCH PAPER

Effect of Magnetic Force on Heat Transfer Increasing in PCM Slurry Flows

Javad Rostami*

Department of Mechanical Engineering, Faculty of Engineering, Razi University, Kermanshah, Iran

Received 16 October 2021;

revised 18 December 2021;

accepted 20 December 2021;

ABSTRACT: The temperature of the phase change material remains almost constant when the phase changes. It means that these materials have a high heat capacity during phase change. This property causes the particles containing these materials to act like distributed heat sinks throughout the field and result in heat transfer increment. However, if these particles are placed inside the thermal boundary layer, they will have a greater impact on the heat transfer rate. The vertical velocity component in the entrance length, prevents particles from being placed near the wall. On the other hand, in this study, the particle coating is iron oxide, which are able to move towards the wall by magnetic force. This magnetic field pulls the particles toward the heated wall and inside the thermal boundary layer. To solve the governing equations, two-phase Eulerian-Lagrangian model has been used. The PCM is Paraffin wax with 30 microns diameter and, particle volume concentration is 10%. This study covers a wide range of Reynolds numbers ($100 < Re < 500$), subcooling numbers up to 0.75 and magnetic field strength (H_0) up to $2.1 \times 10^{-8} \text{ A.m}^{-1}$. The results show 16.56% increase in Nusselt number for $Re=100$ and, $H_0=2.1 \times 10^{-8} \text{ A.m}^{-1}$.

KEYWORDS: micro-encapsulated PCM; Eulerian-Lagrangian, Subcooling number, magnetic field strength.

INTRODUCTION

There are several applications for PCM slurry flow such as: Heat exchangers, solar water heaters, cooling of electronic devices and microchannel heat sinks. The temperature of the phase change material remains almost constant when the phase changes. These particles act as distributed heat sinks and increases the heat transfer coefficient. However, if these particles located inside the thermal boundary layer, they will have a more effects on the heat transfer rate. But, the vertical velocity component in the entrance length, moves particles far from the wall. In this study, the particle coating is iron oxide, which can be conducted towards the wall in presence of magnetic field. This magnetic field pulls the particles toward the heated wall and inside the thermal boundary layer.

Shabgard et al. [1] studied the effects of the solid particle melting in the slurry fluid through the parallel plates on the heat transfer rate numerically. They used the Eulerian-Lagrangian method in the two-way coupling view. The particle concentration exceeds 18%. Their results show that heat transfer rate is proportional to the particle concentration. Seyf et al. [2] investigated heat transfer increments by nano-encapsulated PCM in micro-tubes. In this study, the base fluid was Polyalphaolefin and, the PCM was Octadecane. They reported the pressure loss, heat transfer increment and entropy generation in different Reynolds numbers and various volume fractions. The effects of Brownian motion on freezing of PCM containing nanonoparticles in a cavity studied by Abdollahzade Jamalabadi and Park [3] numerically.

Their simulations were performed in FLUENT software. They showed that due to Brownian motion, the solidification time decreases. Abdollahzade Jamalabadi [4] also, studied the effect of using nanoparticle PCM for cooling of surface acoustic wave sensor. He selected a period of the solution domain and used the periodic boundary conditions. He reported heat transfer improvement up to 10%. Seyyedi et al. [5] studied the effect of inclined magnetic field on the Entropy generation in an annulus filled with NEPCM suspension. The internal pipe is wavy and the external one has elliptic section. The heat transfer mechanism between the two walls was natural convection. The effect of the magnetic field on heat transfer rate of PCM microcapsule suspension has been investigated by Huang et al. [6] experimentally. They showed that applying the magnetic field thinner the thermal boundary layer and increases the heat transfer rate. Hi [7] studied heat transfer during solidification of wavy PCM layers with inclusion of nano-powders in an air flow heat exchanger. The PCM was Paraffin and flow was turbulent. They investigate the heat exchanger operation in presence of nanoparticle and absence of it in the PCM material. Roberts et al. [8] studied the effect of the material type of the micro-capsules shell for cooling the micro-channels. One of the shell material was metal, and another one was nonmetallic material. They concluded that increasing the heat capacity is the main reason of the heat transfer increasing. However, using slurry flow increases the pressure loss, too.

*Corresponding Author Email: rostamij57@gmail.com

Tel.: +989188779216; Note. This manuscript was submitted on October 16, 2021; approved on December 18.

Nomenclature	
a	height of the mini-channel, m
C_p	specific heat capacity, $J.kg^{-1}.K^{-1}$
C_D	Drag Force Coefficient
d_p, D_p	particle diameter, m
F_M	Magnetic force, N
H	magnetic field strength A. m^{-1}
H_0	maximum magnetic field strength A. m^{-1}
h	heat transfer coefficient $W. m^{-2}.K^{-1}$
k	thermal conductivity, $W.m^{-1}.K^{-1}$
L	channel length, m
L_0	Isotherm length, m
L_{sl}	Latent heat of the PCM, $J.kg^{-1}$
m	Mass, kg
n_p	particle number in a cell
Nu	Nusselt number
p, P	non-dimensional and dimensional pressure, Pa
Pe	Peclet number
Pr	Prandtl number
q''	heat flux, $W.m^{-2}$
Re	Reynolds number
Re_p	Particle Reynolds number
Sb	Subcooling number
Ste	Stephane Number
t	time, s
T	non-dimensional temperature
u, v	non-dimensional velocity component in x,y directions
x, y	non-dimensional x,y coordinate
Greek Letters	
α	diffusion coefficient, $m^2.s^{-1}$
δV	The volume of the Eulerian cell, m^3
θ	temperature, K
μ	viscosity, Pa.sec
ρ	density, $kg.m^{-3}$
ϕ	Particle volume concentration
Superscripts	
*	non-dimensional parameters
Subscripts	
b	fluid bulk value, buoyancy
c	cold boundary
C	Particle cover
D	Drag force
f	Fluid
h	hot boundary
i	Internal particle diameter, m
l	Liquid
p	particle
ps	Particle surface
s	Solid
x	Local Nusselt number

The Eulerian-Lagrangian method has been used by [9-13] to study the heat transfer by the nanofluids. Their results show that the two-phase model (Eulerian-Lagrangian) presents closer results to the experiments than the one-phase model. Due to particle distribution, which is not homogenous, causes the one-phase model far from the actual situations.

One way to bring the particles closer to the heated wall and place them in the thermal boundary layer is using magnetic force. This method is used by [14, 15]. Aminfar et al. [14] studied the hydro-thermal behavior of a ferrofluid with 4% spherical Fe_3O_4 nanoparticle in presence of magnetic field numerically. The method was two-phase mixture model. Their results confirm the heat transfer increases in presence of magnetic field. Bahiraei and Hangi [15] studied the effects of magnetic field on the heat transfer rate of magnetic nanofluid in a double-pipe heat exchanger. The nanoparticle in their research was Mn-Zn ferrite. They used two-phase Eulerian-Lagrangian method in their numerical study and considered magnetic force in the particle motion equation. They report the heat transfer increment due to the presence of magnetic field. But, they didn't report detailed results for particle distribution.

To the best of the author's knowledge, there is no study in the PCM slurry flow by Eulerian-Lagrangian method in presence of a magnetic field in a mini-duct. This method has been used in this study to investigate the flow field and heat transfer. The base fluid is water and the PCM is Paraffin-wax

covered by a thin layer of Fe_3O_4 . The particle concentration is 10%, the range of Reynolds number is 100-500, subcooling number is up to 0.75 and magnetic strength from 0 to $2.1e-8 A.m^{-1}$.

GOVERNING EQUATIONS AND BOUNDARY CONDITIONS

Geometry of the mini-channel containing encapsulated micro-sized PCM particles has been defined in [16] and shown in Fig. 1. The height of the mini-channel is 2mm, the length of channel is the length of the fully developed length of the fluid flow.

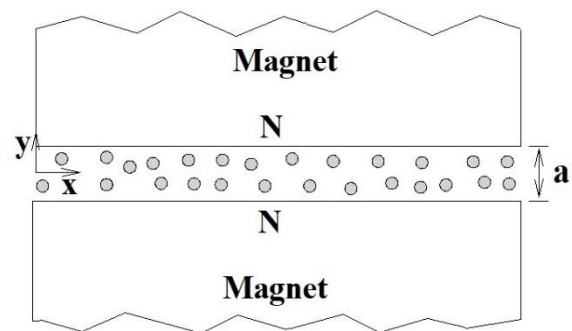


Fig. 1. Geometry of the mini-channel contains microencapsulated PCMs affected by magnetic fields

By introducing the following non-dimensional parameters,

$$\begin{aligned} x_i &= \frac{x_i}{a}, t^* = \frac{U_b t}{a}, u_i = \frac{U_i}{U_b}, p = \frac{P}{\rho_f U_b^2}, \\ T &= \frac{\theta - \theta_c}{\theta_h - \theta_c}, \phi_f = 1 - \phi, Pr = \frac{\mu_f C_p \rho_f}{k_f} \\ Re &= \frac{\rho_f U_b a}{\mu_f}, Pe = Re \cdot Pr, \\ Ste &= \frac{C_p \rho_p (\theta_l - \theta_s)}{L_{sl}}, Sb = \frac{\theta_s - \theta_c}{\theta_h - \theta_c} = T_s \end{aligned} \quad (1)$$

The governing equations are as follows [17],
Continuity,

$$\frac{\partial \phi_f u_i}{\partial x_i} = 0 \quad (2)$$

momentum,

$$\frac{\partial \phi_f u_i u_j}{\partial x_i} = -\frac{\partial \phi_f p}{\partial x_j} + \frac{\partial}{\partial x_i} \left(\frac{\phi_f}{Re} \frac{\partial u_j}{\partial x_i} \right) - \frac{\rho_p}{\rho_f} \frac{\pi d_p^3}{6 \delta V^*} \sum_{np} \frac{du_{pj}}{dt^*} \quad (3)$$

where, the last term in Eq. (3) is created source term by the particles in the Eulerian cell [17] and, np and δV^* are the numbers of particles in the Eulerian cell and, the volume of the Eulerian cell respectively.

Energy,

$$\frac{\partial \phi_f u_i T}{\partial x_i} = \frac{\partial}{\partial x_i} \left(\frac{\phi_f}{Pe} \frac{\partial T}{\partial x_i} \right) - \frac{\pi}{Pe} \frac{d_p}{\delta V^*} \sum_{np} Nu (T_f - T_{ps}) \quad (4)$$

where T_{ps} is the particle surface temperature and “Nu” has been obtained using the following relation [18],

$$h = \frac{k_f Nu}{D_p}, Nu = 2 + 0.6 Re_p^{0.5} Pr^{\frac{1}{3}} \quad (5)$$

The boundary condition for Eqs. (2-4) are presented in [16].

THE PARTICLE PHASE GOVERNING EQUATION IN LAGRANGIAN VIEW

Velocity equations

The velocity governing equation for particles is [19],

$$m_p \frac{dU_p}{dt} = F_D + F_M + F_B + F_g \quad (10)$$

where F_D, F_M, F_B and F_g are Drag force, Magnetic force (Fig. 2), buoyancy force and, weight, respectively.

Due to the equal density of the base fluid and the capsules, the sum of the last two sentences to the right of the Eq. (10) is zero. Based on Fig. 1, in x-direction, just drag force acts on the particles and, there is no magnetic force. The drag

force is due to the velocity difference between the fluid and the particle. By defining C_D as drag coefficient [19],

$$C_D = \frac{18}{Re_p} \frac{\rho_f}{\rho_p} (1 + 0.15 Re_p^{0.687}) \quad (11)$$

the velocity equations of the particles in non-dimensional form is calculated as follows,

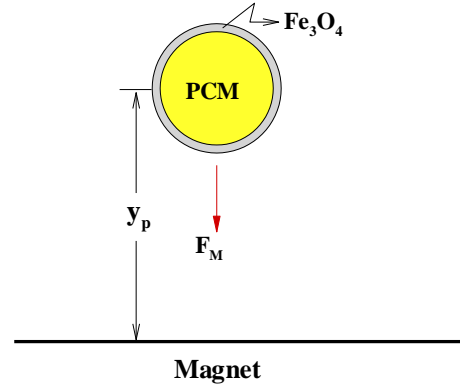


Fig. 2. Magnetic force for a particle

$$\frac{du_p}{dt^*} = C_D (u_f - u_p) \quad (12)$$

where Re_p is defined in [16], based on [17]. Also, in “y” direction,

$$\frac{dv_p}{dt^*} = C_D (v_f - v_p) + \frac{a}{m_p U_b^2} F_M \quad (13)$$

where F_M is defined as follow [20],

$$F_M = \mu_0 (M \cdot \nabla) H \quad (14)$$

where μ_0 is the permeability of vacuum and is equal to $4\pi \times 10^{-7} \frac{H}{m}$, and, “H” is magnetic field strength. The amount of “H” should not be so high that the particles stick to the channel walls. Also, “M” is magnetization and has been obtained by [21], as follows.

$$M = \frac{m}{V_p^0} L(\xi) \quad (15)$$

where V_p^0 is the shell volume and is equal to $\frac{\pi}{6} (D_p^3 - D_i^3)$, and, “m” is magnetic moment and $L(\xi)$ is Langevin function which have been obtained as follow [21],

$$L(\xi) = \frac{1}{\tanh(\xi)} - \frac{1}{\xi} \quad (16)$$

$$\xi = \frac{\mu_0 m H}{k_B \theta} \quad (17)$$

where k_B is Boltzmann constant and is equal to $1.38 \times 10^{-23} \frac{J}{K}$. The unit cell of the crystal structure for Fe_3O_4 has a volume of $730 \times 10^{-30} m^3$ [14] and includes eight molecules. Then the volume of each molecule is equal to $\frac{730}{8} \times 10^{-30} = 91.25 \times 10^{-30} m^3$. Also, magnetic moment for Fe_3O_4 is equal to $4\mu_B$ [22], which, μ_B is Bohr magneton and is equal to $9.27 \times 10^{-24} A.m^2$. Then “m” is obtained as follow,

$$m = \frac{4\mu_B V_p^0}{91.25 \times 10^{-30}} = \frac{4\mu_B}{91.25 \times 10^{-30}} \frac{\pi}{6} a^3 (d_p^3 - d_i^3) \quad (18)$$

Due to the symmetric applied magnetic field, H increases linearly in the “y” direction [20]. Then,

$$H = H_0 \frac{-y}{0.5} = -2H_0 y, \quad y \leq 0 \quad (19)$$

where H_0 is maximum magnetic strength and occurs at the channel wall. Due to Eq. (19) and symmetric geometry, the magnitude of “H” is zero in the channel symmetric line. Then based on Eqs. (1,17-19), in non-dimensional form ξ will obtained as a function of “y”,

$$\xi = -\frac{2\mu_0 H_0}{k_B[(\theta_h - \theta_c)T + \theta_c]} \frac{4\mu_B}{91.25 \times 10^{-30}} \frac{\pi}{6} a^3 (d_p^3 - d_i^3) y \quad (20)$$

Finally, based on Eqs. (13,14,18) the second term of right-hand side of Eq. (12) is equal to,

$$\frac{a}{m_p U_b^2} F_M = -\frac{6\rho_f^2}{\rho_p \pi d_p^3 (\mu Re)^2} \frac{8\mu_0 \mu_B H_0}{91.25 \times 10^{-30}} L(\xi) \quad (21)$$

Energy equation

The properties of water at $40^\circ C$, as the base fluid and Paraffin-wax are given in [16]. The particles elements are 29.75 microns of Paraffin-wax coated with 250 nm thickness of iron oxide (Fe_3O_4). Due to the high Biot number of PCM, the temperature of the particles cannot assume lumped [16]. Then for the particle energy equation, the transient one-dimensional conduction equation is considered [16].

$$\frac{\partial T_p}{\partial t^*} = K \frac{\alpha_p}{\alpha_f} \frac{1}{Pe} \frac{1}{r^{*2}} \frac{\partial}{\partial r^*} \left(r^{*2} \frac{\partial T_p}{\partial r^*} \right) \quad (22)$$

where α is the thermal diffusion coefficient and $K=Ste$ in melting zone and $K=1$ in solid zone temperature.

NUMERICAL PROCEDURE

The fluid flow domain unknowns including velocity components and pressure in the Eulerian view is defined by a finite volume method. To avoid the checkerboard pressure,

the Rhie and Chow [23] interpolation is used. The Hybrid differencing [24] is applied to calculate the convective terms and the well-known SIMPLE method [25] is used to solve the fluid flow domain. The velocity equations of the particles have been solved by the 4th order of the Runge-Kutta method and, their energy equation has been solved by the implicit scheme. To solve the problem, first, the governing equations without particle will be solved, then the particles inject in the domain from the channel inlet. After particles were completely distributed, the governing equation of the particle will be solved and the source terms in Eq. 3 and 4 will calculate. Then the fluid domain will be solved again. These steps continue until the Nusselt number value converge.

RESULTS AND DISCUSSIONS

In this paper heat transfer increasing of slurry flow in a mini-channel, in present of magnetic field, has been studied. The particle diameter is 30 microns and Reynolds numbers differ from 100-500 for particle volume concentrations of 10%, subcooling numbers (0 and 0.75) and magnetic strength from 0 to $2.1e-8 A.m^{-1}$.

Mesh independency have been done in [16] and to avoid duplication, refrain from representing. Due to lack of experimental results, as shown in [16], the results are validated for pure fluid. Also, the particle distributions are in a good agreement with the particle distribution in [9, 15]. Furthermore, to valid the results in the combined hydrodynamics and thermal entrance region, the mean Nusselt number compared with the mean Nusselt number from Ebadian and Dong [26] in Eq. (23), for pure fluid.

$$Nu = 7.55 + \left[\frac{125x^{+1.14} + 4.475Pr^{0.17} x^{+0.5}}{3} \right]^{-1}, \quad x^* = \frac{x}{2Pe} \quad (23)$$

The results show 0.5 % difference between the obtained mean Nusselt number from Eq. (23) and the present code.

Fig. 3, shows the particle distribution in different Reynolds numbers in the absence of magnetic field. The length of the channel has been chosen so that, the flow is fully developed in the channel outlet. In this case, when magnetic field is not applied, the only force on the particles is drag force. In this entrance length, according to the continuity equation, by decreasing the horizontal component of velocity near the wall, the vertical component of velocity is created. This vertical velocity applies the drag force to the particles and sends them away from the wall. However, in terms of heat transfer, the presence of particles near the body is desirable. As mentioned in [16], the PCM particles act as distributed heat sinks in the fluid and reduce the temperature of the surrounding fluid. This increases the heat transfer rate. Fig. 3, shows that, at lower Reynolds numbers, the particles are farther away from the wall. It indicates that the drag force on the particles is lower for higher Reynolds numbers. Because the entrance length is shorter in lower Reynolds numbers. As a result, the velocity developed at a shorter distance, and the changes in the horizontal velocity component (u) are more

significant for low Reynolds numbers. So according to the continuity equation, the vertical component of velocity at the channel inlet is higher for low Reynolds numbers, causing more drag on the particles and driving them further toward the center of the channel. So according to the continuity equation, the vertical component of velocity at the channel inlet is higher for low Reynolds, causing more drag force on the particles and driving them further toward the center of the channel. As a result, we expect, the magnetic force that can overcome the drag force to bring the particles closer to the wall to be greater for low Reynolds numbers.

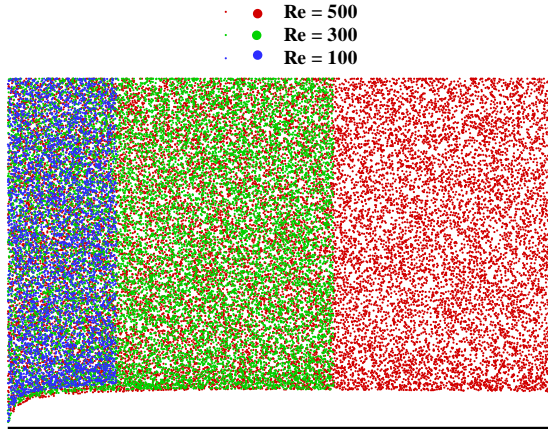


Fig. 3. Particle distribution in different Reynolds number

In fact, the particles appear as heat sinks near the wall or inside the thermal boundary layer and reduce the temperature of the fluid near the body. The purpose of this study is to consider the effect of the conducting particles towards the body using magnetic force on the heat transfer rate. Fig. 4, shows the distribution of particles in different Reynolds numbers in the presence and absence of a magnetic field. As expected and explained in the details of Fig. 3, Re=100 requires a stronger magnetic field to guide particles toward the body. According to Eqs. (20 and 21), at the center of the channel, the magnetic force on the particles is zero.

The closer the particles are to the wall, the greater the magnitude of this force. A limitation that must be considered, is that the particles do not stick to the body. For this reason, there is a limit to the magnitude of magnetic field. So that magnetic force should not be so high that the particles stick to the body. It has been shown in details of Fig. 3, that the intensity required for magnetic field that pulls the particles toward the wall is lower at the higher Reynolds number. Another reason for the lower magnetic field strength at high Reynolds number is that their entrance length is longer. So that magnetic field affects the particle for a longer length, and for the particle not to stick to the wall during the length, magnetic field strength must be less, at high Reynolds numbers. The maximum magnetic field strength for different Reynolds numbers is shown in Table 1.

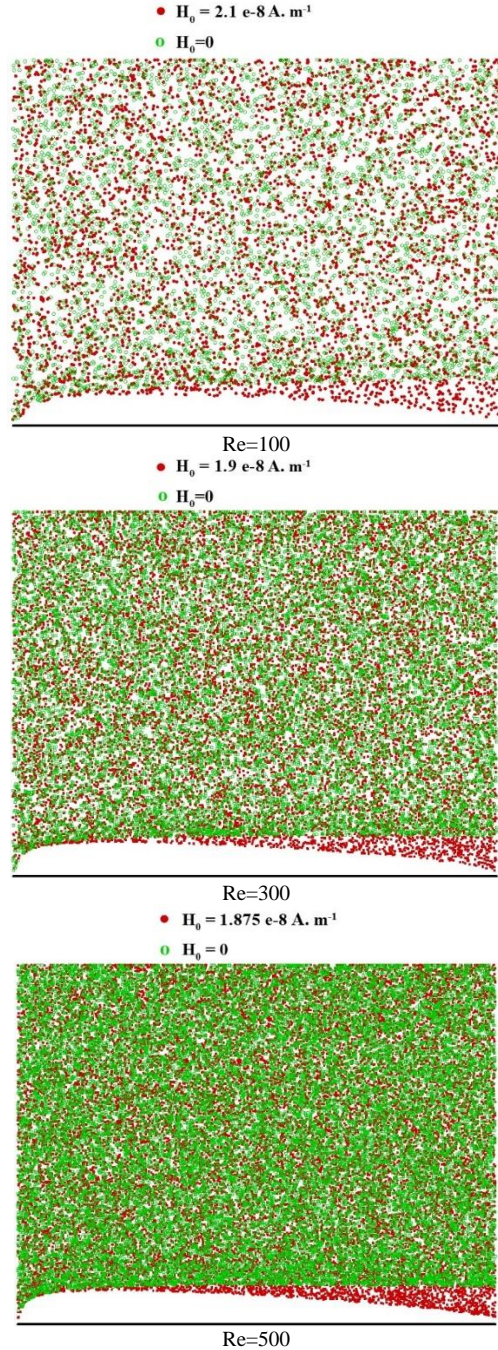


Fig.4. Particle distribution in different Reynolds number with and without magnetic field

Table 1
maximum magnetic field strength in different Reynolds number

			Re
500	300	100	$H_0 (10^{-8} A.m^{-1})$
1.875	1.9	2.1	

It is obtained that, because of observance of particles sticking to the wall, no particle is still placed near the wall at the inlet part of the channel. The particle distribution near the channel outlet is plotted in Fig. 5 for Re=300. It is observed that in the absence of a magnetic field, the particles are far

from the wall. At a distance from the wall, the particle concentration is higher than the average concentration. By applying a magnetic force, the particles are pulled towards the wall, and the distribution of the particles is more uniform than when there is no magnetic field.

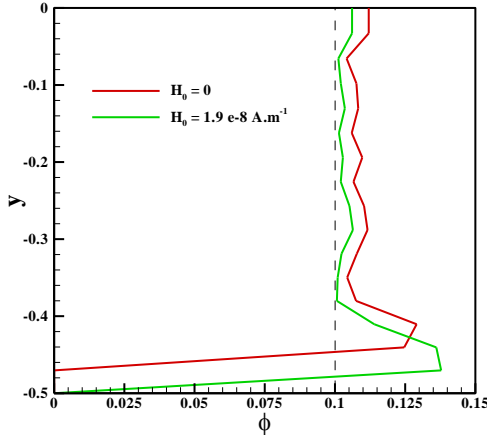


Fig. 5. the particle concentration in presence and absence of magnetic field for Re=300

Fig. 6, shows the effect of the presence of particles in the presence and absence of a magnetic field on the temperature profile near the channel outlet for Re=500. It is observed that the presence of particles has increased the temperature gradient. The application of a magnetic field also increases the slope of the profile.

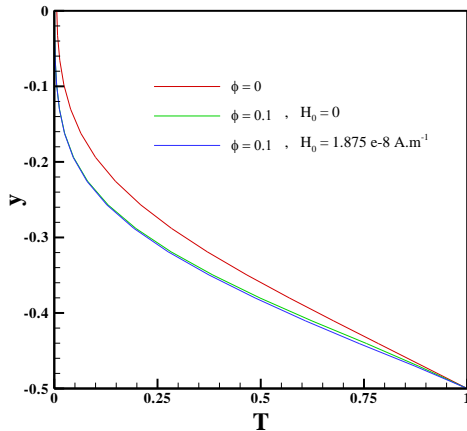


Fig. 6. temperature profile for pure fluid, slurry fluid in presence and absence of magnetic field for Re=500

The effect of applying a magnetic field on the temperature profile for Re=100 has been shown in Fig. 7. The attraction of particles to the body, causes the particles in this range to play the role of heat sinks and reduces the temperature of the fluid near the wall and thus increases the temperature gradient. In this way, the heat flux will be higher in the presence of a magnetic field. However, as seen in Fig. 4, due to the vertical velocity component at the channel inlet and

the large drag force on particles in this area, and, the limited magnitude of the applied magnetic force to prevent the particles sticking to the wall, particles at the beginning of the channel cannot get close to the wall. As a result, the effect of magnetic force from the middle to the end of the channel will gradually show itself.

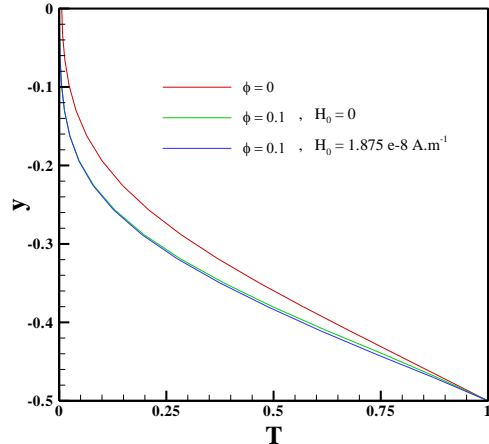


Fig. 7. the particle concentration in presence and absence of magnetic field for Re=300

Fig. 8 shows the local Nusselt number for pure fluid and fluid containing PCM particles in the presence and absence of magnetic field for different Reynolds numbers. It is observed that the presence of particles increases the Nusselt number along the entire length of the channel. The presence of magnetic field also affects the Nusselt number from the middle to the end of the channel, as described in Figs. 4 and 7. Since the length of the solution domain depends on the Reynolds number and varies for different Reynolds numbers, it is not possible to compare the mean values of the Nusselt number for different Reynolds numbers. The resulting increase in Nusselt number for each Reynolds number is compared separately for pure fluid, slurry fluid in the absence of particles, and slurry fluid in the presence of particles and magnetic field in Table 2.

It is observed that the use of microcapsules containing PCM increases the Nusselt number compared to the pure fluid. Using magnetic field according to the above figures causes the particles to be attracted to the body and as a result increases the Nusselt number. Increase in the Nusselt number in the presence of a magnetic field compared to the absence of a magnetic field for Re=100 is 2.09%, for Re=300 is 1.11% and for Re=500 is 1.6%. This result indicates that the effect of the presence of magnetic field is more sensible in the low Reynolds number.

It is observed that the use of microcapsules containing PCM increases the Nusselt number compared to the pure fluid. Using magnetic field according to the above figures causes the particles to be attracted to the body and as a result increases the Nusselt number. Increase in the Nusselt number in the presence of a magnetic field compared to the absence of a magnetic field for Re=100 is 2.09%, for Re=300 is

1.11% and for Re=500 is 1.6%. This result indicates that the effect of the presence of magnetic field is more sensible in the low Reynolds number.

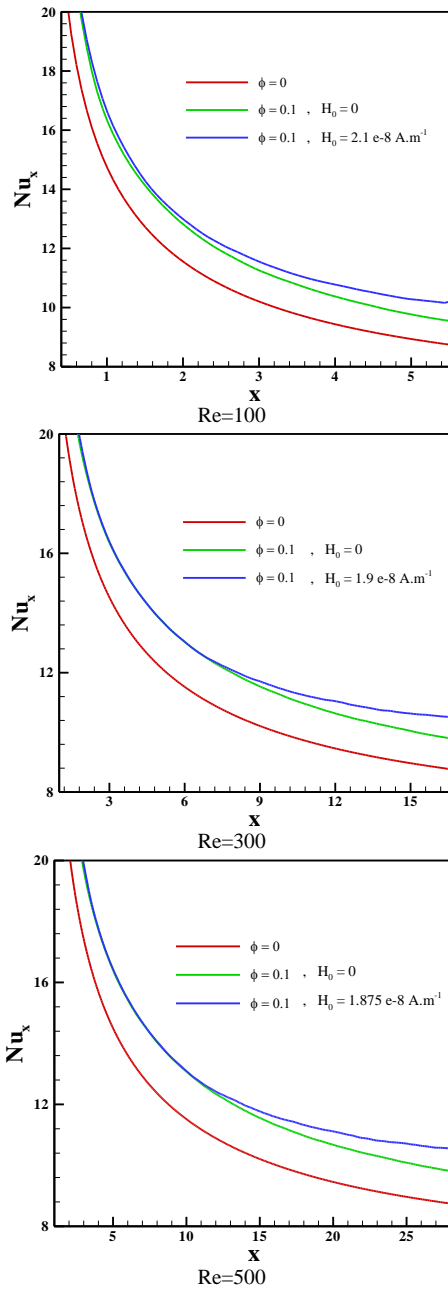


Fig. 8. the local Nusselt number for pure fluid, slurry fluid in presence and absence of magnetic field for different Reynolds numbers.

Table 2

Nusselt number increasing in the absence and presence of Magnetic field

Re	NuPure	NuSlurry	NuMagnet	NuSlurry%	NuMagnet%
100	13.39	15.07	15.35	12.55	14.64
300	14.39	16.40	16.56	13.97	15.08
500	14.26	16.24	16.46	13.85	15.45

The above results were subcooling number equal to zero. In other words, the process of particle melting has started from the beginning of entering the solution zone. But, in some cases, the temperature of the particles entering the solution zone is lower than melting temperature, and the particles enter the solution zone in the solid state. The higher the Sb number, the farther the particle temperature is from their melting temperature. Since the heat capacity of PCM in the solid state is less than the heat capacity of the base fluid, the presence of these particles reduces the heat capacity of the slurry fluid and has a decreasing effect on the Nusselt number. But, when these particles begin to melt, their heat capacity increases dramatically, and in addition to increasing the heat capacity of the slurry fluid, they also act like distributed heat sinks in the fluid [16], cooling the surrounding fluid and increase the Nusselt number.

The presence of a magnetic field pulls the particles towards the wall and close to the thermal boundary layer. The particles approaching the wall cause them to melt due to entering the hot zone. These particles, which begin to melt, affect the rate of heat transfer in two-ways. In the melting state, these particles increase the heat capacity of the slurry flow and simultaneously, appear as heat sinks in the fluid. Fig. 9, shows the ratio of the number of molten particles to the total particles in Re=300 for different Sb number. It is observed that the lower the Sb number, the more particles are melted. By applying a magnetic field to each Sb number, the number of particles in the melting zone increases. For this purpose, the percentage of melted particles is defined as the ratio of the number of particles whose temperature has reached the melting temperature to the total number of the particles as follows.

$$MP = \frac{\text{Number of the melted particles}}{N_p} \quad (23)$$

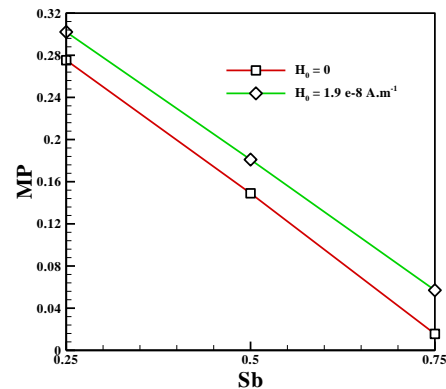


Fig. 9. the melted particles percentage

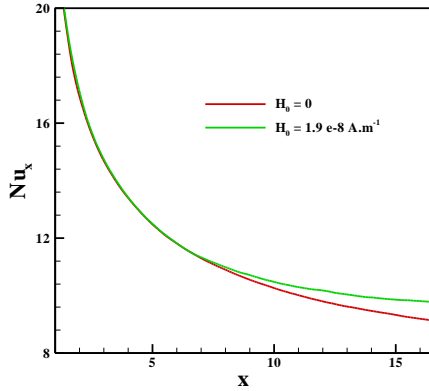


Fig. 10. the local Nusselt number at Re=300 and Sb=0.5 in presence and absence of magnetic field

Fig. 10, also shows the local Nusselt number for Re=300 and Sb=0.5 in the presence and absence of a magnetic field. According to Fig. 9, it can be seen that magnetic field has caused the temperature of more particles to reach the melting zone, and the application of a magnetic field for this state also shows its effect on the Nusselt number from the middle of the channel length.

Fig. 11, also shows the increase of the mean Nusselt number in different Sb numbers. It is observed that the effect of magnetic field for particles with Sb > 0 also has a more significant impact on increasing the mean Nusselt number in lower Reynolds numbers. The higher the Sb number, the less the particles impact on the Nusselt number increasing.

CONCLUSION

The effect of the magnetic fields on the particle motion and their effects on the heat transfer rate for the slurry flow (water containing the micro-encapsulated PCM) through the mini-channel has been studied by the two-phase model in Eulerian-Lagrangian view. The particles are Paraffin-wax covered by a thin layer of Fe₃O₄. The effect of different parameters including Reynolds number, Sb number and different magnetic field strength have been investigated. Results shows, in the absence of magnetic field, due to the vertical component of the fluid velocity in the channel entrance length, particles located far from the hot wall. It causes the particle temperature far from the melting temperature and reduces their role in the heat transfer increasing. But, in presence of magnetic field which pulls these particles toward the heated wall, they participate more in heat transfer increasing. Also, due to preventing particles from sticking to the wall, the intensity of magnetic field cannot be more than a certain amount. On the other hand, the presence of a vertical drag force at the inlet of the channel causes the particles to be gradually pulled towards the wall from the middle of the channel and play the role of a heat sink near the wall from the middle of the channel onwards. This means that the presence of a drag force in the entrance of the channel, limits the increase in Nusselt number.

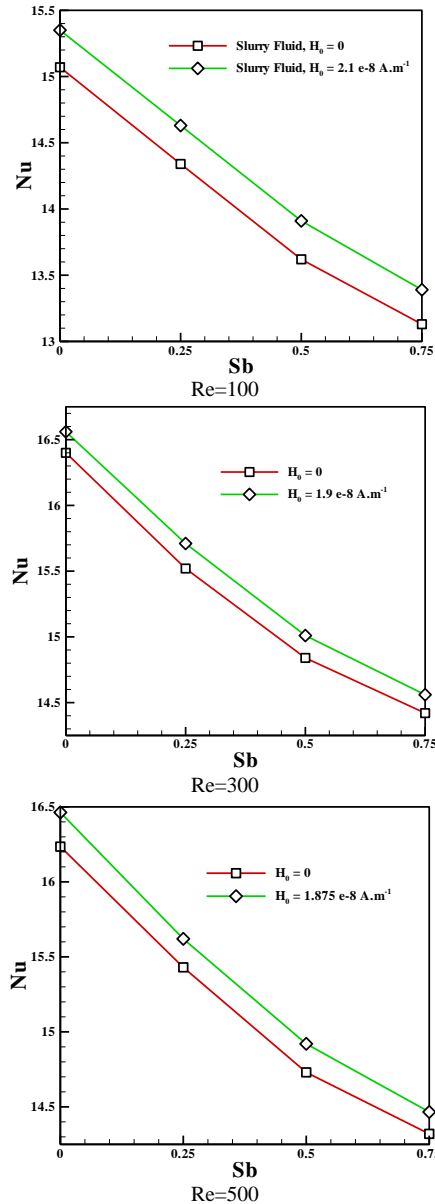


Fig. 11. Mean Nusselt number in different Reynolds number with and without magnetic field vs. Sb number

REFERENCES

- [1] Shabgard H, Hu H, Boettcher PA, McCarthy M, Sun Y. Heat transfer analysis of PCM slurry flow between parallel plates, *International Journal of Heat and Mass Transfer*. 2016; 99: 895-903.
- [2] Seyf HR, Zhou Z, Ma HB, Zhang Y. Three dimensional numerical study of heat-transfer enhancement by nano-encapsulated phase change material slurry in microtube heat sinks with tangential impingement, *International Journal of Heat and Mass Transfer*. 2013; 56: 561-573.
- [3] Abdollahzadeh Jamalabadi MY, Park JH. Effects of Brownian Motion on Freezing of PCM Containing

- Nanoparticles, *Thermal Science*. 2016; 20(5): 1533-1541.
- [4] Abdollahzadeh Jamalabadi MY. Use of Nanoparticle Enhanced Phase Change Material for Cooling of Surface Acoustic Wave Sensor. *Fluids, Thermal Science*. 2021; 6(31), <https://doi.org/10.3390/fluids6010031>.
- [5] Seyyedi SM, Hashemi-Tilehnoee M, Sharifpur M. Effect of Inclined Magnetic Field on the Entropy Generation in an Annulus Filled with NEPCM Suspension, *Mathematical Problems in Engineering*, 2021; <https://doi.org/10.1155/2021/8103300>.
- [6] Huang Y, Xuan Y, Li Q. Experimental investigation on convective heat transfer of magnetic phase change microcapsule suspension, *Applied Thermal Engineering*. 2012; 47: 10-17.
- [7] Li Z. Heat transfer during solidification of PCM layers with inclusion of nano-powders, *International Communications in Heat and Mass Transfer*. 2021; 127: [105518](https://doi.org/10.1016/j.ijheatmasstransfer.2021.105518).
- [8] Roberts NS, Al-Shannaq R, Kurdi J, Al-Muhtaseb SA, Farid MM. Efficacy of Using Slurry of Metal-Coated Microencapsulated PCM for Cooling in a Micro-Channel Heat Exchanger, *Applied Thermal Engineering*. 2017; DOI: <http://dx.doi.org/10.1016/j.applthermaleng.2017.05.001>.
- [9] Mirzaei M, Saffar-Avval M, Naderan H. Heat Transfer Investigation of Laminar Developing Flow of Nanofluids in a Microchannel Based on Eulerian-Lagrangian Approach, *The Canadian Journal of Chemical Engineering*. 2014; 92: 1139-1149.
- [10] Rostami J, Abbassi A, Harting J. Heat Transfer by Nanofluids in Wavy Microchannels, *Advanced Powder Technology*. 2018; 29(4): 925-933.
- [11] Sharaf OZ, Al-Khateeb AN, Kyritsis DC, Abu-Neda E. Direct absorption solar collector (DASC) modeling and simulation using a novel Eulerian-Lagrangian hybrid approach: Optical, thermal, and hydrodynamic interactions, *Applied Energy*. 2018; 231: 1132-1145.
- [12] O. Z. Sharaf, A. N. Al-Khateeb, D. C. Kyritsis, E. Abu-Neda, Numerical investigation of nanofluid particle migration and convective heat transfer in microchannels using an Eulerian-Lagrangian Approach, *Journal of Fluid Mechanics*. 2019; 878: 62-97.
- [13] Sharaf OZ, Al-Khateeb AN, Kyritsis DC, Abu-Neda E. Four-way coupling of particle-wall and colloidal particle-particle interactions indirect absorption solar collectors, *Energy Conversion and Management*. 2019; 195: 7-20.
- [14] Aminfar H, Mohammadpourfard M, Mohseni F. Two-phase mixture model simulation of the hydro-thermal behavior of an electrical conductive ferrofluid in the presence of magnetic fields, *Journal of Magnetism and Magnetic Materials*. 2012; 324: 830-842.
- [15] Bahiraei M, Hangi M. Investigation the efficacy of magnetic nanofluid as a coolant in double-pipe heat exchanger in the presence of magnetic fields, *Energy Conversion and Management*. 2013; 76: 1125-1133.
- [16] Rostami J. Convective Heat Transfer by Micro-Encapsulated PCM in a mini-Duct, *International Journal of Thermal Sciences*. 2021; 161: 106737.
- [17] Minkowycz WJ, Sparrow EM, Murthy JY. 2006, *Handbook of Numerical Heat Transfer*, second ed., John Wiley & Sons, Hoboken, NJ.
- [18] Ranz WE, Marshall WR. *Evaporation from Drops*, *Chemical Engineering Progress*. 1952; 48 (3): 141-146
- [19] Wen D, Zhang L, He Y. Flow and Migration of Nanoparticle in a Single Channel, *Heat and Mass Transfer*. 2009; 45: 1061-1067.
- [20] Zborowski M, Chalmers J. *Magnetic cell separation*, Amsterdam: Elsevier; 2008.
- [21] Yamaguchi H. *Engineering Fluid Mechanics*, 1st ed. Netherlands: Springer; 2008.
- [22] Kittel CH. *Introduction to Solid State Physics*, John Wiley & Sons, New York, 1967.
- [23] Rhie CM, Chow WL. Numerical Study of the Turbulent Flow Past an Airfoil with Trailing Edge Separation, *AIAA J*. 1983; 21(11): 1525-1535.
- [24] Spalding DB. A Novel Finite Difference Formulation for Differential Expressions Involving Both First and Second Derivatives, *International Journal for Numerical Methods in Engineering*. 1972; 4: 551-559.
- [25] Patankar SW, Spalding DB. A Calculation Procedure for Heat, Mass and Momentum Transfer in Three-Dimensional Parabolic Flows, *International Journal of Heat and Mass Transfer*. 1972; 15: 1787-1806.
- [26] Ebdadian MA, Dong ZF. Forced Convection, Internal Flow in Ducts, in: W. M. Rohsenow, J. P. Hartnett, and Y. I. Cho, Eds., *Handbook of Heat Transfer*, McGraw-Hill, New York, 1998.